1-1-2013

Angular rebinning for geometry independent SPECT reconstruction

Alexandre Bousse
University College London

Kjell Erlandsson
University College London

Stefano Pedemonte
University College London

Sebastien Ourselin
University College London

Simon Arridge
University College London

See next page for additional authors

Angular rebinning for geometry independent SPECT reconstruction

Abstract

This work proposes a novel approach to model the collimator response in SPECT. The approach consists of projecting the activity volume on a high number of virtual projection planes that are then averaged with an angular point spread function. It was motivated by the new possibilities offered by GPU for 3-D projection/backprojection. This approach also allows to model a wide range of SPECT imaging systems. Results show that reconstruction using our resolution modelling method is consistent with standard blurring. As an example, we show how to implement a convergent collimator response.

Keywords

rebinning, geometry, angular, independent, reconstruction, spect

Disciplines

Engineering | Science and Technology Studies

Publication Details

Bousse, A., Erlandsson, K., Pedemonte, S., Ourselin, S., Arridge, S. & Hutton, B. F. (2013). Angular rebinning for geometry independent SPECT reconstruction. Fully Three-Dimensional Image Reconstruction in Radiology and Nuclear Medicine 2013 Conference Proceedings (pp. 308-311). Unite States: Fully3d Org.

Authors

Alexandre Bousse, Kjell Erlandsson, Stefano Pedemonte, Sebastien Ourselin, Simon Arridge, and Brian F. Hutton

Angular Rebinning for Geometry Independent SPECT Reconstruction

Alexandre Bousse, Kjell Erlandsson, Stefano Pedemonte, Sébastien Ourselin, Simon Arridge, Brian F. Hutton

***Abstract*—This work proposes a novel approach to model the collimator response in SPECT. The approach consists of projecting the activity volume on a high number of virtual projection planes that are then averaged with an angular point spread function. It was motivated by the new possibilities offered by GPU for 3-D projection/backprojection. This approach also allows to model a wide range of SPECT imaging systems. Results show that reconstruction using our resolution modelling method is consistent with standard blurring. As an example, we show how to implement a convergent collimator response.**

***Index Terms*—SPECT reconstruction, resolution modelling, Hermitian adjoint**

I. Introduction

Single photon emission computed tomography (SPECT) imaging is a routine clinical procedure in nuclear medicine. Accurate image reconstruction requires a precise knowledge of the system matrix *i.e.* the probabilities that a photon emitted from a given position is detected at a given bin. This knowledge depends on several factors, such as the attenuation map [1], [2], the gamma camera geometry and septal penetration [3]. When the system matrix is known, the activity distribution image can be reconstructed by maximising the log-likelihood [4], [5] or penalised log-likelihood [6], [7]. In parallel hole SPECT, it is possible to efficiently project (resp. backproject) the activity distribution (resp. the sinogram) by convolving the activity volume slice by slice by a distant-dependent point spread function (PSF) [2]. This approach usually requires the assumption that the attenuation map within the cone of detection corresponds to the attenuation along the central line.

For other imaging system geometries (convergent SPECT, multi-pinhole, etc.), the above approach is not always feasible and projecting/backprojecting requires the computation of the system matrix. This can be achieved by measuring point source responses [8], [9] or Monte-Carlo simulation [10]–[12]. Obviously, in addition to being unable to incorporate the patient-dependent attenuation map, these approaches are normally too time consuming to be performed on-line.

In this work we propose a 2 step projector that can model a wide range of SPECT imaging systems. The idea was suggested in [13]. The first step consists of projecting the activity distribution on a large number of "virtual" azimuthal and polar angles. This step is performed efficiently using the GPU-accelerated Matlab toolbox NiftyRec [14]. The second step, presented in section II, is a data rebinning operation that takes the form of an angular convolution. Its adjoint operator can be computed so that exact backprojection can be performed. The method does not make use of the central line approximation with respect to the attenuation. In section III two examples of angular PSF are presented: parallel hole and fan-beam geometry. Discussion and conclusion are given in section IV.

Manuscript received February 4, 2013; revised April 16, 2013.

A. Bousse and K. Erlandsson are supported by a centre grant jointly funded by Cancer Research UK (CRUK) and EPSRC. UCLH/UCL receives a proportion of its funding from the UK Department of Health's NIHR Biomedical Research Centre's funding scheme.

A. Bousse, K. Erlandsson and B. Hutton are with Institute of Nuclear Medicine–UCL, University College London, London NW1 2BU, UK. B.F. Hutton is also with the Centre for Medical Radiation Physics at the University of Wollongong, NSW Australia.

S. Pedemonte, S. Ourselin and S. Arridge are with Centre for Medical Image Computing, University College London, London WC1E 6BT, UK.

email: a.bousse@ucl.ac.uk

II. Theory

Let $(\boldsymbol{o}, \overrightarrow{\boldsymbol{x}}, \overrightarrow{\boldsymbol{y}}, \overrightarrow{\boldsymbol{z}})$ be an orthonormal coordinate system in $\mathbb{R}^3$ and $\Omega \subset \mathbb{R}^3$ be the field of view. Without loss of generality we can assume Ω to be the unit ball. The activity distribution can be seen as a function $f(\boldsymbol{r})$ with $\boldsymbol{r} \in \Omega$. The operator $\mathcal{P}$ that maps f into the set of its line integrals is called the *X-ray transform* [15]. The choice of its parametrisation varies across the literature. For this work we define it as follows: let $\mathscr{P}(\varphi, \vartheta)$ be the plane tangent to the unit sphere $\partial\Omega$ at $\boldsymbol{o}(\varphi, \vartheta)$, the point of spherical coordinates $(1, \varphi, \vartheta)$ where $\varphi \in [0, 2\pi[$ is the azimuthal angle and $\vartheta \in [-\pi/2, \pi/2[$ is the polar angle. Let $(\boldsymbol{o}(\varphi, \vartheta), \overrightarrow{\boldsymbol{i}}(\varphi, \vartheta), \overrightarrow{\boldsymbol{j}}(\varphi, \vartheta))$ be a coordinate system on $\mathscr{P}(\varphi, \vartheta)$ such that it coincides with $(\boldsymbol{o}, \overrightarrow{\boldsymbol{x}}, \overrightarrow{\boldsymbol{z}})$ when $\varphi = \vartheta = 0$. The X-ray transform of f on $\mathscr{P}(\varphi, \vartheta)$ at position (x, y) is given by the line integral

$$\mathcal{P}f(x, y, \varphi, \vartheta) = \int_{-\infty}^{+\infty} f(\boldsymbol{p}_{\varphi,\vartheta}(x, y) + t\,\overrightarrow{\boldsymbol{d}}(\varphi, \vartheta))\,\mathrm{d}t \quad (1)$$

where $\overrightarrow{\boldsymbol{d}}(\varphi, \vartheta)$ is the unitary vector normal to $\mathscr{P}(\varphi, \vartheta)$ (pointing to the exterior of Ω) and $\boldsymbol{p}_{\varphi,\vartheta}(x, y)$ is the point of coordinates (x, y) on $\mathscr{P}(\varphi, \vartheta)$ in the $(\boldsymbol{o}(\varphi, \vartheta), \overrightarrow{\boldsymbol{i}}(\varphi, \vartheta), \overrightarrow{\boldsymbol{j}}(\varphi, \vartheta))$ coordinates system. When defined over a set of functions that are square-integrable, $\mathcal{P}$ is a continuous operator (see [15], p. 17). In SPECT imaging, the attenuation map $\mu(\boldsymbol{r})$ is incor-

porated by multiplying $f(\boldsymbol{p}_{\varphi,\vartheta}(x,y) + t\,\overrightarrow{\boldsymbol{d}}(\varphi,\vartheta))$ with $\exp\left(-\int_t^{+\infty}\mu(\boldsymbol{p}_{\varphi,\vartheta}(x,y)+t'\,\overrightarrow{\boldsymbol{d}}(\varphi,\vartheta))\,\mathrm{d}t'\right)$ in (1).

The idea developed here is to re-bin a complete line integral dataset $h(x,y,\varphi,\vartheta) = \mathcal{P}f(x,y,\varphi,\vartheta)$ to model a wide range of imaging systems. Continuous re-binning of $h(x,y,\varphi,\vartheta)$ takes the form of data re-blurring with some weighting function. Assume we wish to model a SPECT gamma camera that rotates around the $\overrightarrow{z}$-axis at a distance ρ to the origin and such that each projection plane is contained in a $[-1,1]^2$ square: the re-binned projection data are obtained by an operator $\mathcal{A}$ defined by

$$\begin{aligned}\mathcal{A}h(x,y,\varphi) &= \int_{-\pi/2}^{\pi/2}\int_0^{2\pi} h(u_{\varphi'}(x),u_{\vartheta'}(y),\varphi+\varphi',\vartheta') \\ &\times\ w(x,y,\varphi',\vartheta')\chi(x,y)\,\mathrm{d}\varphi'\mathrm{d}\vartheta' \qquad (2)\end{aligned}$$

where $u_\delta(t) = \rho\sin\delta + t\cos\delta$, $\chi(x,y)$ is the characteristic function of $[-1,1]^2$ and w is some weighting function. The angular blurring $\mathcal{A}$ can be easily interpreted: at camera position φ and detector bin location (x,y), $\mathcal{A}$ accounts for photons travelling in a direction defined by (φ',ϑ') with a contribution $w(x,y,\varphi,\vartheta)$. The two terms $u_{\varphi'}(x)$ and $u_{\vartheta'}(y)$ indicate where the corresponding photon trajectories are located in the complete dataset $h(x,y,\varphi,\vartheta)$, see figure 1. The geometry of the imaging system is determined by the choice of w. For example, if w does not depend on (x,y), $\mathcal{A}$ models a parallel hole collimator. The theoretical observation operator with angular blurring-based resolution modelling is $\mathcal{H} = \mathcal{A}\mathcal{P}$.

In order to utilise $\mathcal{A}$ for iterative image reconstruction, *i.e.* within an iterative algorithm [4]–[7], its Hermitian adjoint (transpose) must be computed.

Proposition 1. *Let $\mathcal{A}$ be as in (2) and denote $T_1 = [0,2\pi]$ and $T_2 = [0,2\pi]\times[-\pi/2,\pi/2]$. Let X (resp. Y) be the subset of $L^2(\mathbb{R}^2\times T_2)$ (resp. $L^2(\mathbb{R}^2\times T_1)$) composed of functions compactly supported on $[-1,1]^2\times T_2$ (resp. $\mathbb{R}^2\times T_1$). Assume there exists a function $K:\Omega\to\mathbb{R}^+$ such that for all $(x,y)\in[-1,1]^2$, $w(x,y,\varphi,\vartheta)\le K(\varphi,\vartheta)$ and*

$$\sup_{\vartheta,\varphi}\frac{K^2(\varphi,\vartheta)}{|\cos\vartheta\cos\varphi|} = C(w) < +\infty.$$

Then $\mathcal{A}$ is a bounded operator with $\|\mathcal{A}\|\le\pi^{3/2}\sqrt{2C(w)}$ and its adjoint operator $\mathcal{A}^*:Y\to X$ is given by

$$\begin{aligned}\forall g\in Y,\quad \mathcal{A}^*g(x,y,\varphi,\vartheta) &= \int_0^{2\pi} g(v_{\varphi-\varphi'}(x),v_\vartheta(y),\varphi') \\ &\times\frac{w(v_{\varphi-\varphi'}(x),v_\vartheta(y),\varphi-\varphi',\vartheta)}{|\cos(\varphi-\varphi')\cos\vartheta|}\chi(x,y)\,\mathrm{d}\varphi',\end{aligned}$$

where $v_\delta(t) = u_\delta^{-1}(t)$.

Proof. The adjoint is obtained by substituting (x,y) for $v_{\varphi'}(x)$ and $v_{\vartheta'}(y)$ when writing the adjoint equality $\int\mathcal{A}hg = \int h\mathcal{A}^*g$. The division by $|\cos\vartheta\cos\varphi|$ is a Jacobian. The same trick is used to find an upper bound for $\|\mathcal{A}\|$. (Full proof available on demand). □

The condition on w mean trajectories of the photons should not be parallel to the gamma-camera, which is always true. In practice the X-ray transform $\mathcal{P}$ is discretised to a $N\times m$ matrix $\boldsymbol{P} = \mathsf{D}_{N,m}(\mathcal{P})$ where $\mathsf{D}_{\cdot,\cdot}$ is a discretisation operator, and $\mathcal{A}$ is discretised to a $n\times N$ matrix $\boldsymbol{A} = \mathsf{D}_{n,N}(\mathcal{A})$. To perform the angular blurring (2) it is required that $N\gg n$. The full SPECT finite-dimensional projector is a $n\times m$ matrix $\boldsymbol{H} = \boldsymbol{A}\boldsymbol{P}$ and its transpose used for iterative reconstruction is $\boldsymbol{H}^{\mathrm{T}} = \boldsymbol{P}^{\mathrm{T}}\boldsymbol{A}^{\mathrm{T}}$. We utilised $\mathsf{D}_{m,N}(\mathcal{P}^*)\mathsf{D}_{N,n}(\mathcal{A}^*)$ to approximate $\boldsymbol{H}^{\mathrm{T}}$. In section III we demonstrate that $\boldsymbol{H}^{\mathrm{T}}\approx\mathsf{D}_{m,N}(\mathcal{P}^*)\mathsf{D}_{N,n}(\mathcal{A}^*)$. Resolution modelling utilising $\boldsymbol{H}$ and $\boldsymbol{H}^{\mathrm{T}}$ shall be referred to as *angular blurring projection* (ABP). Standard resolution modelling shall be referred to as *standard blurring projection* (SBP) implemented as in [2].

Because $N\gg n$ (*i.e.* high number of virtual projections), $\boldsymbol{P}$ and $\boldsymbol{P}^{\mathrm{T}}$ should be implemented efficiently. For this work we utilised the GPU-accelerated Matlab toolbox NiftyRec [14].

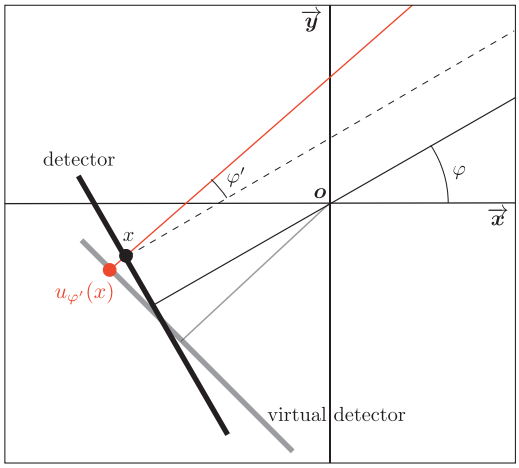

Fig. 1. Illustration of the angular re-binding: $u_{\varphi'}(x)$ is the virtual camera detection location of a photon hiting the true camera at angular position φ at location x with an angle φ'.

III. Results

A. Validation of the adjoint operator

In this section we experimentally verify that $\mathsf{D}_{m,M}(\mathcal{A}^*)\approx\boldsymbol{A}^{\mathrm{T}}$. This is can be considered as an experimental verification of proposition 1. For this purpose we randomly generate two sequences $\{\boldsymbol{u}_k\}$ and $\{\boldsymbol{v}_k\}$ where $\boldsymbol{u}_k\in\mathbb{R}^n$ and $\boldsymbol{v}_k\in\mathbb{R}^N$, $N\gg n$. For each k, we verify that

$$\langle\boldsymbol{A}\boldsymbol{u}_k,\boldsymbol{v}_k\rangle_{\mathbb{R}^N}\approx\langle\boldsymbol{u}_k,\mathsf{D}_{N,n}(\mathcal{A}^*)\boldsymbol{v}_k\rangle_{\mathbb{R}^n}. \qquad (3)$$

Figure 2 shows that (3) is a good approximation.

B. Imaging system examples

In this section we show 2 examples of SPECT systems: parallel hole and convergent cone-beam collimators. As briefly explained in section II, parallel hole collimators can be modelled with ABP using a position-independent PSF. Here we used a two-dimensional Gaussian PSF with diagonal covariance matrix *i.e.*

$$w_{\mathrm{par}}(\varphi,\vartheta)\propto\chi_R(\varphi,\vartheta)\exp(-\varphi^2/2\sigma_\varphi^2)\exp(-\vartheta^2/2\sigma_\vartheta^2) \qquad (4)$$

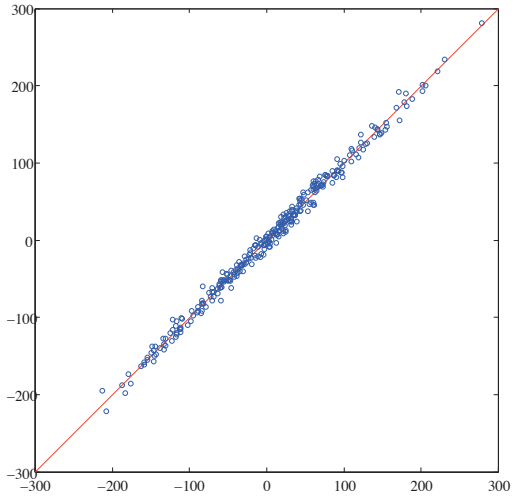

Fig. 2. Plot of 300 points whose coordinates are the left and right hand side of (3).

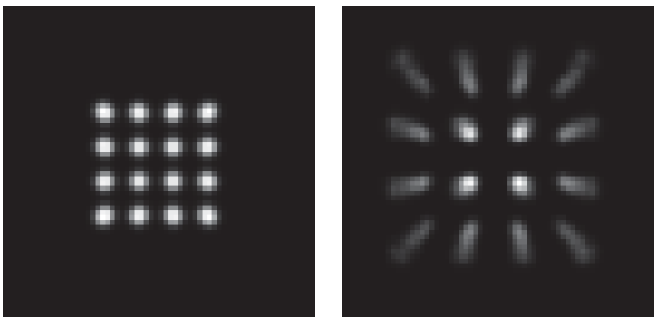

(a) w_{par} (b) w_{conv}

Fig. 3. Projection with resolution modelling following (2): (a) parallel hole collimator *i.e.* using (4); (b) convergent fan-beam collimator *i.e.* using (5)

where R is such that $d(R, \{-\pi/2, \pi/2\}) > 0$ and χ_R is the corresponding characteristic function. The presence of χ_R is necessary to ensure the hypothesis of proposition 1 is true *i.e.* by excluding angles $\pm\pi/2$. The convergent and divergent geometry PSF's are built upon w_{par} with the introduction of a term that changes the angular centring depending on the position (x, y) on the camera:

$$w_{\text{conv}}(x, y, \varphi, \vartheta) = w_{\text{par}}(\varphi + x\varphi_{\max}, \vartheta + y\vartheta_{\max}). \quad (5)$$

We chose a linearly-dependent position centring but other position dependencies can be used. Note that divergent geometries can be implemented by replacing $\varphi_{\max}$ and $\vartheta_{\max}$ with $-\varphi_{\max}$ and $-\vartheta_{\max}$ respectively. Figure 3 shows the results of noiseless projection using parallel hole (figure 3(a)) and convergent geometry (figure 3(b)). The projected phantom consists of 64 spheres distributed uniformly in a cube. The volume size is $m = 64^3$ and the projection data size is $n = 64^2 \times 120$. We used 360 virtual azimuthal angles φ and 360 polar angles ϑ to compute $\mathcal{A}$ (*i.e.* $N = 64^2 \times 360^2$). With parallel geometry only the first layer is visible, whereas using convergent geometry the 3 next layers are visible.

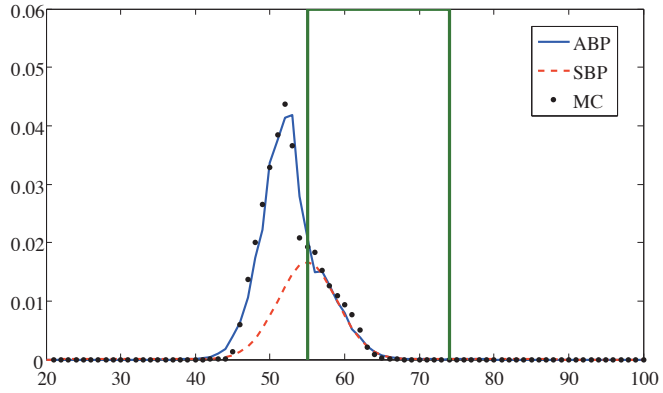

Fig. 4. Projected point source section using ABP and SBP projector and MC. The rectangle represents the border of the attenuation medium.

C. Monte-Carlo simulations

1) Point source in attenuated medium: We projected a simulated point-source located in a rectangular phantom containing water with the Monte-Carlo (MC) code SIMIND [16], as well as using SBP and ABP. The point-source was purposely located at the border of the attenuation medium in order to assess the effect of the central line approximation. A section of the projected point-source is shown in figure 4. It shows that the central line approximation results in an evenly distributed projected point-source using SBP, whereas the projected point source using ABP is similar to the MC projection.

2) Phantom evaluation: We evaluated our new projector/back-projector using simulated data. MC SPECT projection data were generated using SIMIND. The activity distribution was a cylinder (28 cm diameter) containing 4 cylindrical inserts of different sizes (diameters from 35 to 56 mm). The true contrast in all spheres compared to the background was 3. Simulations were done corresponding to a rotating scintillation camera equipped with a LEHS collimator with a radius of rotation of $\rho = 192\,\text{mm}$. The number of projection angles over 360° was 120 ($n = 120 \times$ number of pixels/projection). The effects of scatter were not simulated. The object central slice was reconstructed in 2-D with ABP and SBP. ABP was performed using 720 azimuthal polar virtual angles ($N = 720 \times$ number of pixels/projection). Activity images were reconstructed with a surrogate based algorithm [7] with a quadratic smoothing prior weighted by a parameter β. We used 3 different values of the regularisation parameter β.

The reconstructed images were assessed by their mean contrasts in each cylinder as well as coefficient of variation (COV) calculated across 10 MC realisations. Reconstructed images using SBP and ABP are shown in figure 5(a) and 5(b) respectively. The 2 images appear similar although a weak dark ring can be seen in the SBP reconstructed image close to the edge of the phantom, probably due to inaccurate attenuation modelling. Figure 6 shows the COV vs contrast curves of the penalised maximum

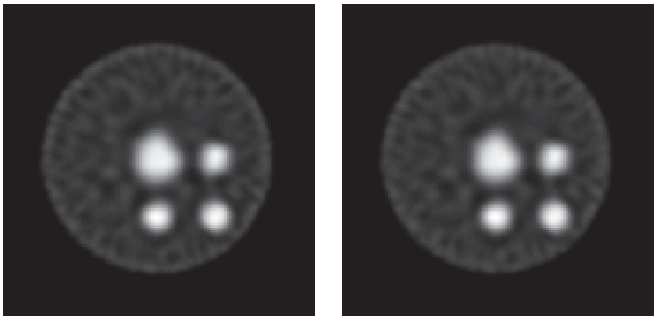

(a) SBP reconstruction (b) ABP reconstruction

Fig. 5. Reconstruction from MC data: (a) using SBP; (b) using ABP.

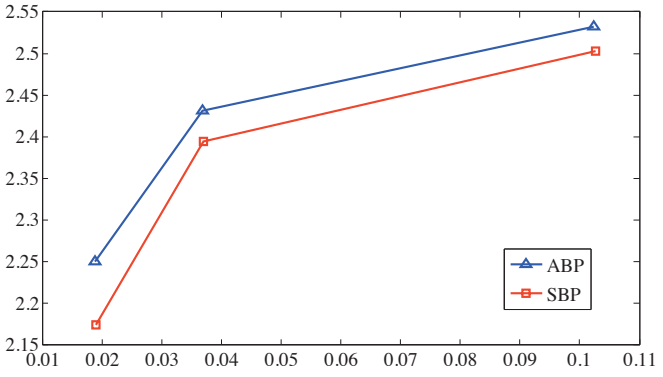

(a) 400 iterations

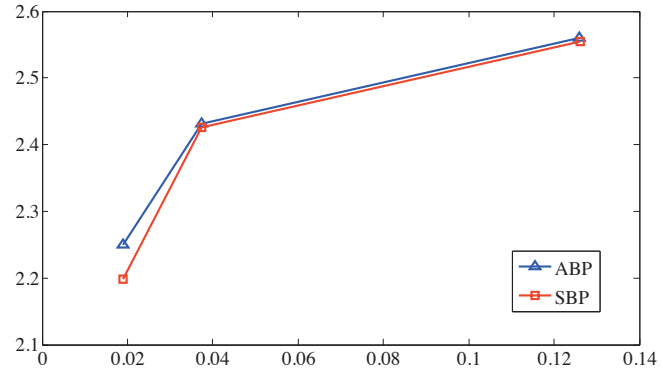

(b) 600 iterations

Fig. 6. Penalised-ML reconstruction contrast vs COV for 3 different values of β: (a) 400 iterations; (b) 600 iterations.

likelihood (ML) reconstructed images using SBP and ABP for 3 values of β after 400 iterations (figure 6(a)) and 600 iterations (figure 6(b)). The contrast was calculated over the bottom right disk. Although results are very similar after 600 iterations, ABP reconstruction performs better than SBP when only 400 iterations are performed.

IV. Discussion and conclusion

Here we have presented a new projection/back-projection technique for SPECT reconstruction, which is based on an angular blurring approach instead of the traditional distance dependent blurring approach. Our new method utilises the speed-up obtained with a GPU-device for parallel-beam forward and back-projection, and has a high degree of flexibility, allowing a wide range of collimators to be modelled by simply changing a weighting function. Here we have illustrated the flexibility of the method and we have shown that it produces results similar to the traditional approach. In further work we intend to model a wider range of imaging systems and optimise their performances.

Acknowledgment

The authors would like to thank Michael Ljungberg and Maria Holstensson for help with running SIMIND.

References

[1] G. T. Gullberg, R. H. Huesman, J. A. Malko, N. J. Pelc, and T. F. Budinger, "An attenuated projector-backprojector for iterative spectreconstruction," *Phys. Med. Biol.*, vol. 30, no. 8, pp. 799–816, 1985.

[2] G. L. Zeng, C. Bai, and G. T. Gullberg, "A projector/backprojector with slice-to-slice blurring for efficient three-dimensional scatter modeling," *IEEE Trans. Med. Imag.*, vol. 18, no. 8, pp. 722–732, 1999.

[3] L. Lin, P. L. Kench, M.-C. Gregoire, and S. R. Meikle, "Projection process modelling for iterative reconstruction of pinhole SPECT," *IEEE Trans. Nucl. Sci.*, vol. 57, no. 5, pp. 2578–2586, 2010.

[4] L. A. Shepp and Y. Vardi, "Maximum likelihood reconstruction for emission tomography," *IEEE Trans. Med. Imag.*, vol. 1, no. 2, pp. 113–122, 1982.

[5] K. Lange and R. E. Carson, "EM reconstruction algorithms for emission and transmission tomography," *J. Comput. Assist. Tomo.*, vol. 8, no. 2, pp. 306–316, 1984.

[6] P. J. Green, "Bayesian reconstruction from emission tomography using a modified EM algorithm," *IEEE Trans. Med. Imag.*, vol. 9, no. 1, pp. 84–92, 1990.

[7] A. R. de Pierro, "A modified expectation maximization algorithm for penalized likelihood estimation in emission tomography," *IEEE Trans. Med. Imag.*, vol. 14, no. 1, pp. 132–137, 1995.

[8] R. K. Rowe, J. N. Aarsvold, H. H. Barrett, J. C. Chen, W. P. Klein, B. A. Moore, I. W. Pang, D. D. Pattonand, and T. A. White, "A stationary hemispherical SPECT imager for three-dimensional brain imaging," *J. Nucl. Med.*, vol. 34, no. 3, pp. 474–480, 1993.

[9] F. van der Have, B. Vastenhouw, M. Rentmeester, and F. J. Beekman, "System calibration and statistical image reconstruction for ultra-high resolution stationary pinhole SPECT," *IEEE Trans. Med. Imag.*, vol. 27, no. 7, pp. 960–971, 2008.

[10] M. Rafecas, B. Mosler, M. Dietz, M. Pogl, A. Stamatakis, D. P. McElroy, and S. Ziegler, "Use of a Monte Carlo-based probability matrix," *IEEE Trans. Nucl. Sci.*, vol. 51, no. 5, pp. 2597–2605, 2004.

[11] D. Lazaro, Z. el Bitar, V. Breton, D. Hill, and I. Buvat, "Fully 3D Monte Carlo reconstruction in SPECT," *Phys. Med. Biol.*, vol. 2005, pp. 3739–3754, 2005.

[12] Z. el Bitar, Y. Petegnief, D. Lazaro, D. Hill, V. Breton, and I. Buvat, "Targeted fully 3D Monte Carlo reconstruction in SPECT," in *IEEE Nucl. Sci. Symp. Conf. Record,*, vol. 6, 2006, pp. 3414–3419.

[13] A. S. Fokas, B. F. Hutton, and K. Kacperski, "Modeling of collimator in analytical SPECT image reconstruction," internal report.

[14] S. Pedemonte, A. Bousse, K. Erlandsson, M. Modat, S. Arridge, B. F. Hutton, and S. Ourselin, "GPU accelerated rotation-based emission tomography reconstruction," in *IEEE Med. Imag. Conf. Record*, 2010, pp. 2657–2661.

[15] F. Natterer, *The Mathematics of Computerized Tomography*. Society for Industrial and Applied Mathematics, 2001.

[16] M. Ljungberg and S.-E. Strand, "A Monte Carlo program simulating scintillation camera imaging," *Comput. Methods Programs Biomed.*, vol. 29, pp. 257–272, 1989.